# Aerodynamic assessment of potential rudder force augmentation due to circulation control based on a VTP rudder design for a STOL aircraft

**By D. Keller AND R. Rudnik†**

Institut für Aerodynamik und Strömungstechnik, Deutsches Zentrum für Luft- und Raumfahrt
Lilienthalplatz 7, 38108, Braunschweig

The scope of the paper is to assess the potential of using circulation control at the vertical tail plane in order to increase the maximum rudder side force. Therefore, a numerical study on the rudder design is carried out, consisting of a 2D sensitivity study, an estimation of the 3D forces and moments via lifting line method, and a verification by 3D Reynolds-averaged Navier-Stokes (RANS) simulations. Compared to the baseline rudder, the lifting line method yields a $138\%$ increase of the rudder yawing moment due to the use of circulation control. 3D RANS simulations verify the lifting line results. The deviation between yawing moments from the RANS computations and the lifting line method is less than $11\%$.

## 1. Introduction

Applying circulation control on high-lift configurations is a promising approach to reduce emissions and travel time as it may allow the use of short runways and thus to utilize existing aerospace infrastructure more efficiently. The principal potential of such systems is already well known [1]. It's potential for the present configuration is assessed within the research project. Additional lift benefits can be obtained by slipstream-main wing interaction due to wing mounted turboprop engines. The combination of an active high-lift system in conjunction with propeller induced lift augmentation was already studied by NASA [2, 3] in the sixties and seventies of the last century and by TsAGI [4]. However, these studies and associated ones [5] also revealed challenges regarding flight mechanical properties. The most severe ones are related to the lateral motion and in particular to the case of an engine failure. With the numerical approach, as applied in the Collaborative Research Center *SFB 880*, it was possible to reproduce the aerodynamic phenomena, which cause the negative effects in lateral motion [6] and gain a better understanding of the underlying complex wake flow topology. Even though, the work also resulted in measures, which potentially reduce the negative effects, the aircraft configuration poses high demands on the necessary control forces.
The presented paper assesses the potential of using circulation control in order to enhance the maximum rudder side force. Therefore, a numerical study on the rudder design is carried out. In the first step, basic design parameters of the slot geometry and

† Institut für Aerodynamik und Strömungstechnik, Deutsches Zentrum für Luft- und Raumfahrt, Braunschweig

| | |
|---|---|
| Reference area | $27\mathrm{m}^2$ |
| Span | $5.692\mathrm{m}$ |
| Aspect ratio | $1.2$ |
| Sweep angle | $35^\circ$ |
| Mean aerodynamic chord | $4.759\mathrm{m}$ |
| Rudder length | $4.84\mathrm{m}$ |

TABLE 1. Basic geometric parameters of the VTP

the rudder are investigated based on a 2D sensitivity study. Then, the results of the 2D study are used to estimate the potential rudder forces and moments with an extended non-linear lifting line method. In the last step, the results from the lifting line method are verified with 3D Reynolds-averaged Navier-Stokes (RANS) computations of the full aircraft.

## 2. Numerical method

### 2.1. *RANS computations*

The calculations are performed with the *DLR TAU* code [7], which is based on an unstructured finite volume approach for solving the RANS equations. For this investigation, the implicit LUSGS scheme is used for time stepping and a central scheme for the spatial discretization of the convective fluxes. The turbulence effects are modeled with the original Spalart-Allmaras formulation [8] with vortical and rotational flow correction based on the Spalart-Shur correction [9].

### 2.2. *Extended non-linear lifting line*

The preliminary estimation of the vertical tail plane (VTP) forces and moments is carried out with an extended non-linear lifting line method. The method is similar to Van Dam's and Wickenheiser's modified Weissinger method [10, 11] and combines the improvements from Weissinger's extended lifting line method with an iterative procedure to account for non-linear viscous effects. Therefore, the method uses 2D sectional data, which can be derived from various sources.

## 3. Geometric model

The control surface design is based on the REF2-2013 aircraft configuration [12], which resulted from a preliminary design process carried out with PrADO [13]. Details on the geometric model of the landing configuration, which is used for the RANS simulations can be found in [6]. Details on the basic geometric parameters of the VTP are summarized in Table 1. The baseline rudder has a conventional layout with a relative rudder depth of $c_R = 0.396$.

The computational mesh of the full model for the RANS simulations was created by a semi-automated hybrid meshing approach [14] and consists of two overlapping blocks, which are connected by a chimera approach. The combined mesh consists of 107 to 117 million points, depending on the considered VTP rudder.

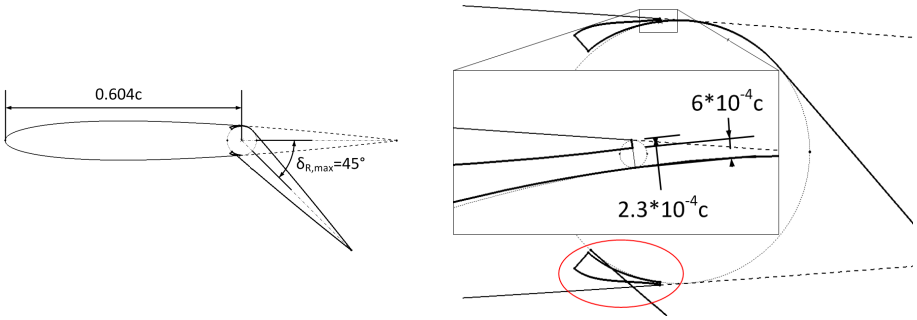


(a) Overview (b) Detail at the rudder hinge line position

FIGURE 1. VTP section

## 4. Results

### 4.1. *Sectional data*

The flight dynamic simulations yielded exceptionally high requirements regarding maximum rudder forces, which can be mainly attributed to the large yawing moments, that are necessary to trim the aircraft with one engine inoperative. As a result, it is questionable if a conventional rudder can deliver sufficiently large side forces while maintaining a reasonable VTP and rudder size. Therefore, the use of circulation control at the VTP is investigated, since it promises higher maximum side forces. However, compared to the application at the main wing, the use of circulation control is more challenging, since the rudder deflects in both directions and therefore, the system has to work symmetrically, as well. Figure 1(a) sketches the VTP airfoil geometry with an rudder length of $c_R = 0.396$, as it was defined for the baseline rudder without circulation control. The sketch shows the centric hinge line position and the two plena symmetrically located below and above the hinge point. If the slot exit geometry is designed with the conventional approach for asymmetric control surface deflections, the rudder would collide with the main element in case of moderate to large deflection angles. This is demonstrated in figure 1(b), which shows the region at the rudder's hinge line position in detail. Therefore, the slot exit geometry has to be modified to avoid the collision and to allow rudder deflections in both directions. One approach to do this is to cut back the main element's trailing edge, as it is shown in figure 2(a). The size of the cut back is dependent on the maximum possible rudder deflection. The higher the maximum deflection is the larger the cut back has to be. Here, a cut back for a maximum rudder deflection of $\delta_{R,max} = 45°$ is shown, which results in a trailing edge thickness of $l_{TE} = 5.22 * 10^{-3}c$. Another approach is to remain the trailing edge thickness and to introduce a step between the rudder surface and the slot exit, as it is shown in figure 2(b). For the same maximum rudder deflection of $\delta_{R,max} = 45°$, the step size has to be $l_{Step} = 2.87 * 10^{-3}c$ in order to avoid the rudder collision. Adding the step size to the trailing edge thickness of $l_{TE} = 2.3 * 10^{-4}c$ yields a combined thickness of $l_{TE+St} = 3.1 * 10^{-3}c$. Consequently, the approach with the step leads to a smaller region of potential flow re-circulation at the slot exit at the same maximum rudder deflection angle.

Figure 3 shows the results of an analysis of the influence of the cut backs on the side force coefficient $C_{SF}$ with respect to the sideslip angle $\beta$ for the case of $\delta_R = 45°$ and $C_\mu = 0.035$. Compared to the baseline geometry, which is represented by the black

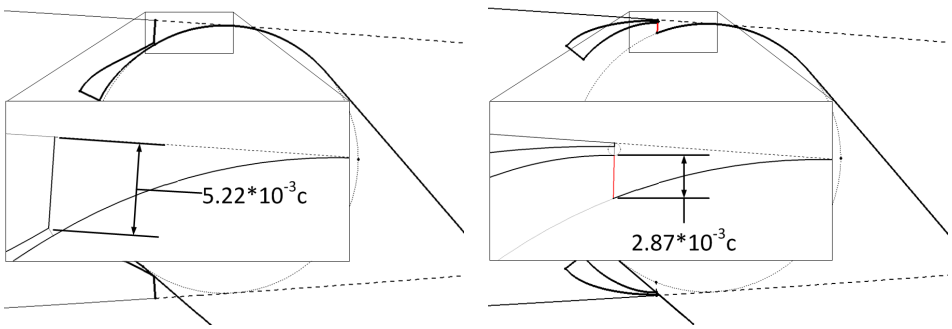


(a) large trailing edge (b) with step

FIGURE 2. Slot exit geometry for symmetric blowing slots

line, the geometries with the cut back in terms of large trailing edge (red line) or step (blue line) both yield smaller maximum side forces. However, the reduction in maximum side force in case of the large trailing edge is with $\frac{\Delta C_{SF,max,lTE}}{C_{SF,max,baseline}} = -12.2\%$ significantly larger than it is for the step geometry with $\frac{\Delta C_{SF,max.Step}}{C_{SF,max,baseline}} = -5.4\%$. The difference is less in the linear region. At $\beta = -15°$, the difference is $\frac{C_{SF,lTE}}{C_{SF,baseline}} = -7.5\%$ compared to $\frac{C_{SF,Step}}{C_{SF,baseline}} = -3.0\%$. Furthermore, while both geometry adaptions increase the maximum sideslip angle, the thick trailing edge leads to a larger increase. The worse performance of the large trailing edge geometry compared to the step geometry can be fully accounted to the quantitative increase of the cut back. If the length of the large trailing edge would be equal to the combined length of the step ($c_{lTE} = 3.1 * 10^{-3}c$), which is represented by the green line, the performance of the geometry would be also nearly identical with the performance of the step geometry. However, in this case, the maximum rudder deflection would be smaller.
Another important aspect of the geometry design is its influence on drag in cruise conditions. A rough estimation of the additional drag based on 2D simulations yielded an increase in drag of $\Delta C_D = 0.00005$ on aircraft level, if the baseline airfoil contour is modified by introducing the slots with steps. For comparison, the additional aircraft drag compared to the baseline geometry is $\Delta C_D = 0.00002$, if the circulation control slots are integrated without cut backs.

Due to the superior performance of the step geometry, this approach is adopted for further studies on the VTP rudder design. The aim of the design is to maximize the VTP's side force at the lowest possible amount of blowing. Therefore, figure 4(a) illustrates the trends of a rudder length variation in terms of side force generation with respect to the side slip angle at a constant blowing rate of $C_\mu = 0.022$ for the baseline rudder deflection $\delta_R = 40°$. It shows that for small rudder lengths, the maximum side force increases with rising rudder length. However, at some point, which is $c_R = 0.3$ under these conditions, the maximum side force begins to decrease if the rudder length is further enlarged. The reason for this is an altered flow topology at the flap. While the flow remains fully attached to the flap until $\beta_{max}$ is reached at small rudder lengths, it begins to separate from the flap at lower sideslip angles in case of the large rudder. Therefore, large rudder lengths shift the begin of the less effective super-circulation regime to higher momentum coefficients and promise higher potential maximum side forces at good efficiency. But

for moderate blowing rates, they might yield a lower maximum side force than smaller rudders do. However, the sideslip angle, at which the necessary maximum side force is needed is dependent on the dimensioning case, which determines the force requirements. In the case of the REF2-2013 configuration, the necessary VTP rudder side force is prescribed by the yawing moment, which is necessary to make heading changes of $15°$ with the wings level and an one engine inoperative condition. Since the necessary side force is expected to be exceptionally large, the VTP's circulation and with it, the side wash will be large as well. Based on preliminary lifting line calculations, the local sideslip angle in case of a flight without sideslip will be $\beta_{local} \lesssim -15°$ for a large proportion of the VTP span. Therefore, it seems more important to focus on the trends in the linear region of the side force curve. Here, the side force coefficient keeps rising with increased rudder length even at $c_R = 0.396$. Consequently, it can be concluded that a long rudder is more favorable for an efficient maximum side force than a short rudder.

The most influential parameter regarding side force generation is the rudder deflection. Figure 4(b) compares the influence of the rudder deflection angle on the side force generation for the baseline case and for the case with circulation control. Here, the selected blowing rates are the least necessary ones in order to maintain the flow fully attached to the rudder at $\beta = 0°$. For the baseline cases, which are represented by the dashed lines, the side force coefficient generally increases with the rudder deflection. However, at $\delta_R = 30°$ and very low sideslip angles, the flow is attached to the rudder in contrast to the higher deflection angles. Therefore, the side force slope is larger and the side force becomes bigger than for higher deflection angles. At $\beta = 10°$, the flow suddenly separates from the rudder and the side force breaks down. Afterwards, it continues to increases with rising sideslip angle, even though at a lower gradient. With rising incidence angle, the side force increments due to the rudder deflection become less since the flow is already completely separated from the rudder. While the side force coefficient for $\delta_R = 40°$ is still larger than the one for $\delta_R = 30°$ at the maximum sideslip angle, it is reduced if the rudder deflection is further raised to $\delta_R = 60°$. Activating circulation control increases the side force generation substantially in the linear region as well as at the maximum sideslip angle, whereas the increase is dependent on the deflection angle. At $\delta_R = 30°$, the difference in maximum side force coefficient yields $\Delta C_{SF,30} = 0.80$ or $\Delta C_{SF,30}/C_{SF,30,BSL} = 39.3\%$. With rising deflection angle, the additional maximum side force due to circulation control increases to $\Delta C_{SF,60} = 2.60$ or $\Delta C_{SF,60}/C_{SF,60,BSL} = 127.1\%$. In the linear region, the side force is also considerably raised. However, the maximum sideslip angle is continuously reduced due to circulation control and with rising deflection angle. The reason for this is the leading edge geometry. The nose shape is the limiting factor for the maximum side slip angle. The small nose radius leads to a strong leading edge suction peak and a large adverse pressure

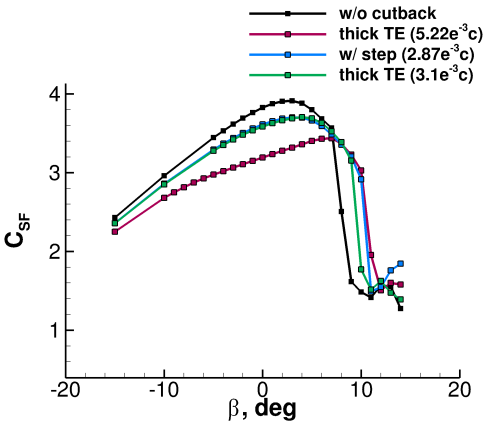


FIGURE 3. Influence of slot exit geometry on side force generation at $\delta_R = 45°$ and $C_\mu = 0.035$

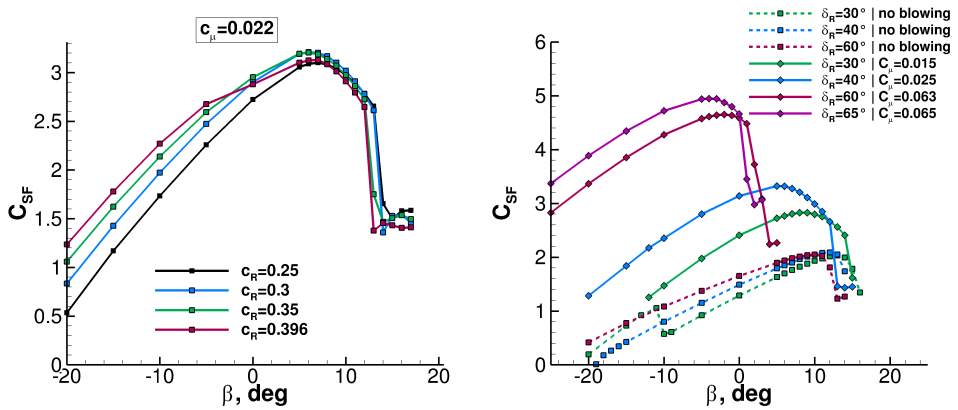


(a) Influence of rudder length at $\delta_R = 40°$ and $C_\mu = 0.022$

(b) Influence of deflection angle and circulation control at $c_R = 0.396$

FIGURE 4. Sideforce creation with respect to sideslip angle

gradient, thereafter. The accompanied momentum losses within the boundary layer result in a wake burst above the rudder, which limits the maximum sideslip angle. With rising deflection angle, the leading edge suction peak and the resulting adverse pressure gradient increases at constant sideslip angle. Therefore, the wake burst occurs at lower sideslip angles.

Figure 4(b) also demonstrates that the deflection angle, which leads to the maximum sideslip angle, is raised due to circulation control. While the maximum deflection angle is $\delta_R \leq 60°$ in the baseline case, a deflection angle of $\delta_R = 65°$ still promises further lift increases in case of activated circulation control. However, it has to be kept in mind that the increase of the deflection angle will eventually lead to reduced efficiency, since the cut back at the main element's trailing edge has to be increased.

### 4.2. *Lifting line*

Considering the geometric properties of the VTP, the estimation of the VTP's yawing moment is expected to be a very challenging case for the lifting line method. With an aspect ratio of $AR = 1.2$, the VTP has a very small aspect ratio. Furthermore, in t-tail configuration, the HTP acts as a huge wing tip device at the VTP tip. At the lower side, the VTP is affected by the fuselage and its boundary layer. All these aspects are not properly represented by the used lifting line method. Nevertheless, it is expected that the method will deliver a better approximation of the 3D VTP side forces, yawing and rolling moments than 2D sectional data will do.

Figure 5 shows the side force distributions along the VTP span $\eta_{VTP}$, which were derived from the lifting line method based on the 2D sectional data. In the lower part at $\eta_{VTP} \lesssim 0.2$, the side force is small and widely constant as it represents the fuselage. At mid-board between $0.2 \lesssim \eta_{VTP} \lesssim 0.88$, the side forces are the highest due to the rudder. In the outboard region at $\eta_{VTP} \gtrsim 0.88$, no rudder exists. Therefore, the load is reduced, here. The plot confirms the basic trend seen in the sectional data. Thus, the increase of the rudder deflection from $\delta_R = 30°$ to $\delta_R = 40°$ increases the side force distribution in both cases without circulation control (dashed lines) and with circulation control (solid lines), whereas the increase is larger in case of activated circulation control. Further-

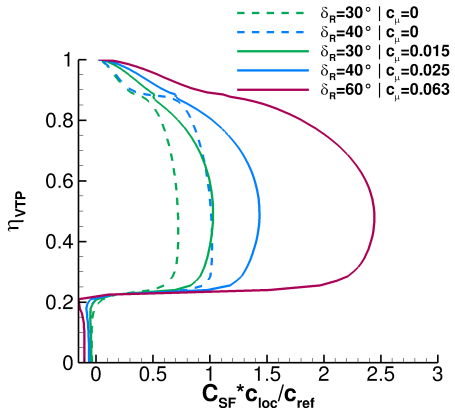


FIGURE 5. Sideforce distribution along VTP span at $\beta = 0°$

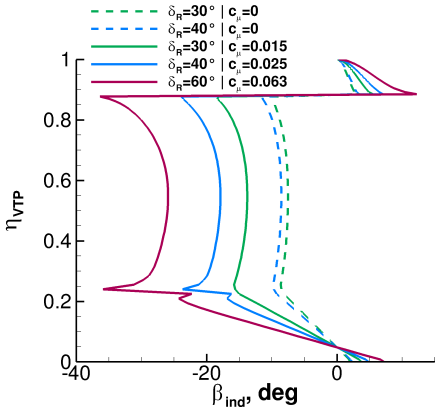


FIGURE 6. Induced sidewash distribution along VTP span at $\beta = 0°$

more, the use of circulation control itself notably increases the side force distribution. However, the magnitudes of the local side forces are significantly lower than the ones seen in the sectional data at $\beta = 0°$ even at the location of the mean aerodynamic chord $\eta_{VTP,MAC} = 0.61$, where $c_{loc} = c_{ref}$. The reason is the strong local sidewash due to the large gradients of the circulation distribution, which results from the high load and the low aspect ratio of the VTP. Figure 6 compares the local sidewash angle distribution along the VTP span. In the region of the rudder, negative sidewash angles exists, whereas the level depends on the VTP load. While they are still moderate with $\beta_{ind} > -10°$ in the baseline cases without circulation control, the local sidewash angle becomes as large as $|\beta_{ind}| > 30°$ for the case with circulation control and $\delta_R = 60°$ rudder deflection.

The lifting line method also yields the resulting yawing moments due to rudder deflection $\Delta C_{Mz,R}$, which are summarized in table 2. The listed yawing moments are calculated as the differences of the total yawing moments of the VTP and the yawing moments of the VTP without any rudder deflection. At $\beta = 0°$, the maximum yawing moment of the baseline rudder is $\Delta C_{Mz,R} = -0.24$. At the same rudder deflection of $\delta_R = 40°$, the rudder with circulation control can already increase the yawing moment by $42\%$ to $\Delta C_{Mz,R} = -0.34$. In this case, the momentum coefficient for the VTP circulation control system with respect to the aircraft reference area is expected to be $C_\mu = 0.006$. However, the yawing moment can be further increased if the rudder deflection is increased. At $\delta_R = 60°$, the VTP yields $\Delta C_{Mz,R} = -0.57$, which would be an increase of $138\%$. Furthermore, the yawing moment seems less sensitive to the sideslip angle in case of a rudder with circulation control. In contrast, it significantly decreases between $-10° < \beta < 0°$ at $\delta_R = 30°$ of the baseline configuration. The reason is that the flow is still attached to the rudder in the underlying 2D simulations for low sideslip angles, yielding higher side forces as seen in figure 4(b).

Due to the large requirement on the necessary rudder yawing moment, the aim of applying circulation control to the rudder was to increase its side force creation. However, circulation control could be also potentially used to reduce the VTP size, if the maximum necessary rudder side force is moderate and the determining factor for the VTP size. Additional lifting line calculations yielded a potential VTP size reduction of $22\%$ for the REF2-2013 configuration, if the baseline rudder was substituted by a rudder with

| Case | $\delta_R$ | $C_\mu$ | $\Delta C_{Mz,R}$ $\beta = -10°$ | $\beta = 0°$ | $\beta = 10°$ |
|---|---|---|---|---|---|
| BSL | 30° | - | -0.35 | -0.17 | -0.12 |
| BSL | 40° | - | -0.30 | -0.24 | -0.16 |
| CC | 30° | 0.0036 | -0.25 | -0.24 | -0.22 |
| CC | 40° | 0.0060 | -0.34 | -0.34 | -0.32 |
| CC | 60° | 0.0153 | -0.60 | -0.57 | -0.52 |

TABLE 2. Yawing moment due to rudder deflection

circulation control, a maximum deflection angle of $\delta = 40°$ and a global momentum coefficient of $C_\mu = 0.0047$. At a maximum rudder deflection of $\delta_R = 45°$ and a momentum coefficient of $0.006$, the size reduction is $30\%$. Based on the results, it is expected that the VTP size could be further reduced if the maximum rudder deflection is increased. However, increasing the maximum rudder deflection reduces the efficiency due to an increased cut back at the slot exit and increases the jet momentum requirements.

### 4.3. *3D RANS simulations*

In order to verify the results from the preliminary rudder design, 3D RANS computations of the full aircraft with rudder deflection were carried out. The initial simulations were performed at $\alpha = 0°$, $\beta = 0°$, $C_{\mu,WING} = 0.03$ and no thrust. Figure 7 compares the flow topology at the VTP of the baseline case at $\delta = 30°$ (figure 7(a)) and the case with circulation control at $\delta_R = 60°$ (figure 7(b)). In the baseline case, the flow is almost completely separated from the rudder in the upper half, as it is indicated by the streamlines. Towards the fuselage, the flow is fully attached to the rudder. In the case with circulation control, the flow is fully attached to the rudder even at high rudder deflections, such as $\delta_R = 60°$. Table 3 summarizes the resulting VTP yawing moments due to rudder deflection at $\alpha = 0°$ and $\beta = 0°$. The baseline case at $\delta_R = 30°$ yields a yawing moment, which is $29\%$ higher than estimated by the lifting line method. The reason for the large difference is that the flow is partially attached to the rudder in the result of the RANS computation, as seen in figure 7(a). The lifting line method also reproduces the VTP's attitude of being close to the point of beginning rudder separation. This is evidenced in the strongly reduced yawing moments at $\beta = 0°$ compared to $\beta = -10°$. At $\beta = -3°$, the yawing moment due to the rudder still is $\Delta C_{Mz,R} = -0.21$. The deviations of the baseline case at $\delta_R = 40°$ and cases with circulation control at $\delta_R = 40°$ and $\delta_R = 60°$ are $11\%$, $8\%$ and $10\%$, respectively. In all cases, the lifting line method underpredicts the yawing moment except for the case of $\delta_R = 60°$. However, in this case, the momentum coefficient is significantly lower in the RANS computations. Therefore, the deviation of the yawing moment will be even less, if the blowing rate is adapted.

Obviously, a rudder deflection also leads to rolling moments. This usually is unwanted, since the rolling moments have to be balanced out by the ailerons. Table 3 also compiles the rolling moments for the computed cases. For example, the rudder with circulation control leads to a notable rolling moment of $\Delta C_{Mx,R} = 0.08$ at a rudder deflection of $\delta_R = 60°$. Assuming a reasonable rolling moment derivative due to aileron deflection of

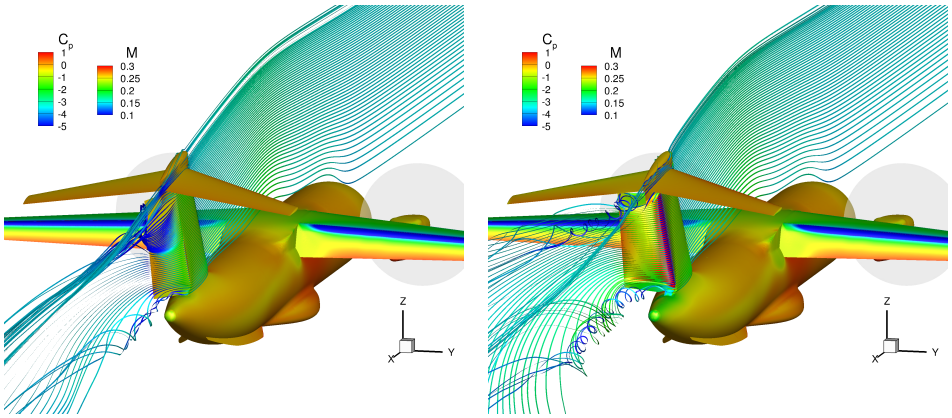


(a) Baseline with $\delta_R = 40°$ (b) $\delta_R = 60°$ with circulation control

FIGURE 7. Surface pressure distribution and streamlines at $\alpha = 0°$ and $\beta = 0°$

| Case | $\delta_R$ | $C_\mu$ | $\Delta C_{Mx,R}$ | $\Delta C_{Mz,R}$ |
|---|---|---|---|---|
| BSL | 30° | - | 0.03 | -0.22 |
| BSL | 40° | - | 0.04 | -0.27 |
| CC | 40° | 0.005 | 0.06 | -0.37 |
| CC | 60° | 0.011 | 0.08 | -0.52 |

TABLE 3. VTP yawing moment due to rudder deflection at $\beta = 0°$

$C_{Mx\xi} = -0.3$, the ailerons would have to be deflected by $\pm 15°$ in order to compensate the rolling moment due to rudder deflection.

## 5. Conclusion

The paper documents the large potential of using circulation control at the VTP in order to enhance rudder force creation. Therefore, a stepwise aerodynamic design study is presented. A 2D sensitivity study demonstrates the impact of the slot exit design for symmetric rudders with circulation control. Furthermore, the impact of the necessary trailing edge cut back on the cruise drag is assessed. Based on the results of the 2D sensitivity study, the geometric design of the slot exit and the rudder was chosen and then evaluated via lifting line method.

The lifting line method yields a $138\%$ increase of the yawing moment due to the use of a circulation controlled rudder. In order to create an equal yawing moment as the baseline rudder does, the VTP size can be reduced by $22\%$ at a momentum coefficient of $C_\mu = 0.0047$. The VTP size could be further reduced, if higher rudder deflections and therefore higher momentum coefficients are chosen.

In order to verify the lifting line results, 3D RANS computations of the full aircraft in landing configuration with rudder deflection were carried out. Except for the baseline case with a moderate rudder deflection, the deviations of the yawing moments were less than $11\%$. Therefore, it is shown that the design approach based on a 2D RANS

computations in conjunction with a lifting line method is well suited for the preliminary estimation of forces and moments of highly loaded rudders with circulation control.

## References


[1] KORBACHER, G. K. (1974). Aerodynamics of powered high-lift systems. *Annual Review of Fluid Mechanics*, **6**, 319–358.

[2] GRIFFIN, JR., R. N. AND HOLZHAUSER, C. A. (1958). Large-scale wind-tunnel tests of an airplane model with an unswept, aspect-ratio-10 wing, two propellers, and blowing flaps. *NASA Memorandum*, **12-3-58A**.

[3] WEIBERG, J. A. AND HOLZHAUSER, C. A. (1961). STOL characteristics of a propeller-driven, aspect-ratio-10 wing, straight-wing airplane with boundary-layer control flaps, as estimated from large-scale wind-tunnel tests. *NASA Technical Note*, **D-1032**.

[4] PETROV, A. (2012). Aerodynamics of STOL airplanes with powered high-lift systems. In: *Proceedings of the ICAS 2012 Congress*, Brisbane, Australia.

[5] QUIGLEY, H. C. AND INNIS, R. C. (1963). Handling Qualities and Operational Problems of a large Four-Propeller STOL Transport Airplane. *NASA Technical Note*, **D-1647**.

[6] KELLER, D. AND RUDNIK, R. (2016). Numerical Investigations of Aerodynamic Properties of a Propeller Blown Circulation Control System on a High Wing Aircraft. *CEAS Aeronautical Journal*, **7**(3), 441–454.

[7] GERHOLD, T. (2005). Overview of the Hybrid RANS Code TAU. *Notes on Numerical Fluid Mechanics and Multidisciplinary Design*, **89**, 81–92.

[8] SPALART, P. R. AND ALLMARAS, S. R. (1992). A One–Equation Turbulence Model for Aerodynamic–Flows. *AIAA Paper*.

[9] SPALART, P. R. AND SHUR, M. (1997). On the sensitization of turbulence models to rotation and curvature. *Aerospace Science and Technology*, **1**(5), 297–302.

[10] VAN DAM, C. P., VANDER KAM, J. C. AND PARIS, J. K. (2001). Design-Oriented High-Lift Methodology for General Aviation and Civil Transport Aircraft. *Journal of Aircraft*, **38**(6), 1076–1084.

[11] WICKENHEISER, A. M. AND GARCIA, E. (2011). Extended Nonlinear Lifting-Line Method for Aerodynamic Modeling of Reconfigurable Aircraft. *Journal of Aircraft*, **48**(5), 1812–1816.

[12] WEISS, T. W. AND HEINZE, W. (2013). Multidisciplinary Design of CESTOL Aircraft with Powered Lift System. *TU Braunschweig - Campus Forschungsflughafen, Berichte aus der Luft- und Raumfahrttechnik*, **2013-3**.

[13] HEINZE, W., ÖSTERHELD, C. M. AND HORST, P. (2001). Multidisziplinäres Flugzeugentwurfsverfahren PrADO - Programmentwurf und Anwendung im Rahmen von Flugzeug-Konzeptstudien. *Jahrbuch der DGLR-Jahrestagung 2001 in Hamburg*.

[14] CENTAURSOFT (2012). Centaur Hybrid Grid Generation System. [online web site], URL: http://www.centaursoft.com.